Grain boundary motion assisted via radiation cascades in bcc Fe

Carlos Campañá and K. P. Boyle
CANMET-Materials Technology Laboratory, Natural Resources Canada, Ottawa, Ontario, Canada K1A 0G1

Ronald E. Miller*
Department of Mechanical and Aerospace Engineering, Carleton University, Ottawa, Ontario, Canada K1S 5B6
(Received 30 July 2008; revised manuscript received 12 October 2008; published 31 October 2008)

Molecular-dynamic simulations were performed to study the influence of displacement cascades on grain boundary (GB) structure and stability in bcc Fe. A $\Sigma=5$, (310)[001] symmetric tilt boundary with a tilt angle of $\theta=36.9°$ was used for the simulations. We find that GB motion, either sliding or migration, is activated under the influence of displacement cascades at lower internal stresses as compared to the unirradiated GBs. We postulate that radiation-induced GB damage aids the nucleation mechanisms that trigger GB motion. Furthermore, radiation-induced GB sliding significantly relaxes internal stress and may provide a viable mechanism for promoting irradiation creep via GB accommodation processes.

DOI: 10.1103/PhysRevB.78.134114 PACS number(s): 61.80.−x, 61.72.Mm, 02.70.Ns

I. INTRODUCTION

Understanding the stability of materials exposed to radiation is a high priority task for the nuclear industry. To fulfill the goal of constructing the next generation of nuclear reactors, extensive materials selection, development, and performance evaluation are required as material degradation may potentially limit the various reactor designs being considered. In particular, materials used in the reactor core must be able to withstand more severe radiation dosages, temperatures, and pressures as compared to current reactors.[1,2]

Advanced steels hold promise for use in these next generation nuclear reactors as they are suitable for use at relatively high temperature and pressure and have proven somewhat resistant to radiation-induced swelling.[3] However, steels are generally susceptible to radiation damage in the form of radiation-induced embrittlement and irradiation creep.[4] Experimental studies are therefore required to assess and understand these phenomena. Nevertheless, such studies are expensive in terms of time and resources due to the inherent difficulty of handling irradiated materials and the wide range of time and length scales associated with radiation-induced damage processes.

Fortunately, various aspects of radiation-induced damage and creep can now be studied with a high degree of realism using multiscale computational techniques.[5,6] Virtual experiments enable the investigation of phenomena not amenable to experimental study and can be used to guide material design. Displacement cascades, the fundamental radiation damage inducing event in materials, are not amenable to experimental study as they have a lifetime of a few picoseconds and cannot be observed directly by experiment. However, displacement cascades lead to the production of defects which evolve over time and lead to changes in microstructure and macroscopic properties. Due to the importance of understanding the primary radiation damage event, molecular-dynamics computations have been extensively used to study displacement cascades in metals, primarily in bcc Fe (Refs. 7–13) although fcc and hcp materials have also been studied. Recent review articles[11,14–16] summarized the state of the field and the influence of variables such as interatomic potential, temperature, radiation dosage, and simulation technique on defect production and clustering. Current research focuses on developing realistic interatomic potentials[17,18] and understanding the influence of solute on primary defect production, primarily in Fe-based alloys.[19,20]

The majority of primary radiation damage computational studies reported in the literature focus on characterizing the changes in the properties of the bulk and stress-free lattices and largely ignore the influence of grain boundaries and interfaces. However, grain boundaries and interfaces are important for mediating plastic deformation and play an important role in many aspects of creep. In the present work, we investigate the combined influence of radiation and internal stress on the stability of grain boundaries in bcc Fe. We have chosen a well-characterized bicrystal for this purpose; i.e., a $\Sigma=5$, (310)[001] symmetrical tilt grain boundary.

The remainder of the paper is organized as follows. In Sec. II, we describe the technical details related to the molecular-dynamics (MD) simulations and chosen bicrystal geometry. In Sec. III, we quantify the irradiation defects produced by direct radiation of the grain boundaries and compare the results to the defects produced by bulk irradiation. We also investigate how internal stress influences the grain boundary displacement cascade events. Last, in Sec. IV our findings are summarized and the implication of our results with regards to irradiation creep are discussed.

II. METHOD

To study the short time scale associated with primary neutron irradiation damage of materials, we have chosen a molecular-dynamics approach. All simulations were performed with LAMMPS, a simulation package distributed by Sandia National Laboratories.[21,22] Our interest in understanding the mechanical stability of irradiated grain boundaries (GBs) in metallic systems motivated us to consider pure bcc Fe $\Sigma=5$, (310)[001] symmetric tilt bicrystals. This tilt geometry allowed us to benchmark some of the results presented in this work with those of a previous study performed on identical crystalline structures.[23] The tilt angle in these sys-

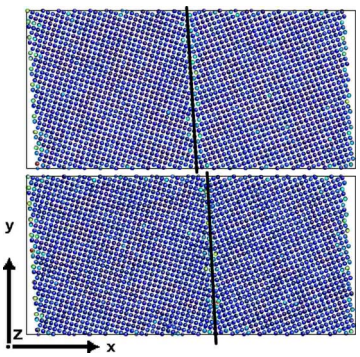

FIG. 1. (Color online) Configurations of a bcc Fe $\Sigma=5$, (310)[001] symmetric tilt bicrystal strained along xy. The top configuration represents the initial bicrystal. The bottom configuration shows the bicrystal 20 ps after a GB displacement cascade, initiated with a PKA energy of 1 keV. GB migration can be identified by comparing the initial and final positions of the GB (tilted straight line).

tems is $\theta=36.9°$ and the [001] tilt direction of the bicrystal was oriented parallel to the z axis of the simulation box (see Fig. 1).

The minimum-energy structure for a given bicrystal is computed by generating an initial set of configurations such that rigid-body translations are applied to the crystal on opposite sides of the GB.[24] This procedure creates bicrystals in which the crystal lattice located on one side of the boundary is shifted in the GB plane with respect to the crystal lattice on the other side. Next, a conjugate gradient minimization technique[25] is used to relax each configuration while looking for the one with minimum energy. This lowest energy configuration is later used as the initial structure for all MD simulations presented. For the above calculations, periodic boundary conditions were considered in all spatial dimensions and the orientation of the unstrained GBs was parallel to the yz planes following the axis convention displayed in Fig. 1.

To avoid potential artifacts introduced to the atomic equations of motion by a thermostat, our systems are set to satisfy the statistics of the microcanonical ensemble (NVE). The reason for considering only NVE ensembles stems from the fact that, to the best of our knowledge, there is no general consensus when it comes to selecting a thermostat able to properly describe electronic heat conduction within metallic structures. Interesting contributions have been proposed to model electronic heat transport in metals,[26–28] although agreement on a well-suited implementation for such purposes has not yet been reached. Finite temperatures are accounted for by setting the initial atomic velocities such that they follow a Maxwell-Boltzmann distribution. All simulations were initialized to a temperature of 300 K.

The atoms within the crystals interact via the embedded atom method (EAM) potential developed by Mendelev *et al.*[29] This potential has proven to be well suited for the description of Fe and has been employed to simulate liquid-solid interfaces. Nevertheless, in order to use the tabulation of EAM formulation of Mendelev *et al.*[29] provided in LAMMPS to study primary displacement cascades with energy higher than 2 keV, one needs to modify it slightly. Specifically, the tabulation of the pair potential packaged with LAMMPS is truncated below $r_0=0.5$ Å, but high primary knock-on atom (PKA) energies can temporarily bring atoms into very close proximity at the start of the simulation. As such, it is necessary to extrapolate the potential to smaller r values to avoid numerical problems. To achieve such a goal, we have used an extrapolation technique based on fitting $\phi(r)$ to a rational function of the form $R(r)=Q(r)/P(r)$. Here $Q(r)$ and $P(r)$ are polynomials of degree $n>9$. For a given order k of the rational polynomial $R(r)$ (typically $k\geq 6$), we make sure that such a function perfectly fits the closest $k+1$ values of the Mendelev potential to where the singularity lives ($r_0=0.5$ Å). Thus, for distances $r'\leq r_0$ the values of the newly tabulated potential correspond to those obtained after evaluating $R(r')$. For $r'>r_0$ the tabulation remains identical to the tabulation Mendelev *et al.* As we are only concerned with simulations corresponding to neutron irradiation of at most 5 keV, the new set of pair values $\{r', R(r')\}$ to be added to the tabulation of Mendelev *et al.* is certainly very small and are accessed predominantly during the very early stages of the simulation. As such, we don't expect our *ad hoc* extrapolation technique to compromise the accuracy of the results to be presented in the next section.

Imposing external strain (stress) on the bicrystal is achieved by independently tilting the simulation box along the xy, xz, or yz planes. As opposed to the work of Hyde *et al.*[23] and Qi and Krajewski,[30] we have chosen to strain the bicrystal at the start of the simulations rather than to apply shearing forces on the outermost atomic layers. An approximation of this type represented more closely the strained (stressed) conditions crystalline grains are exposed to in the experimental setups we were interested in modeling. The simple shear strain $\gamma_{\alpha\beta}$ applied to the simulation box is chosen to be a multiple of γ_0, i.e., $\gamma_{\alpha\beta}=2\gamma_0$, $4\gamma_0$, $5\gamma_0$, etc., where $\gamma_0=\delta/L_0=1/128\approx 0.007\,81$. Here, L_0 is the undeformed length of the box along one of the principal axes on the shearing plane and δ the corresponding relative displacement. After applying the initial strains, the crystals are relaxed for 20–40 ps and the stress tensor $\sigma_{\alpha\beta}$ is monitored to ensure that among the nondiagonal components, only the one along the shearing plane is different from zero. In our displacement cascade simulations, the intrinsic stress threshold for activating GB motion[30] is not exceeded for any of the initial configurations.

It should be mentioned that our approach for straining the simulation box leads to nonzero diagonal components of the stress tensor at $t=0$. However, such components remain small as compared to the primary shear stress responsible for driving the GB motion. For example, an initial internal stress of $\sigma_{xz}=3.8$ GPa leads to diagonal stresses given by $\sigma_{\alpha\alpha}\approx 500$ MPa or about 13% of σ_{xz}. The previous $\sigma_{\alpha\alpha}$ refers to each independent diagonal component of the stress tensor such that Einstein's summation convention is not assumed over repeated indices.

The effects of bombarding the bicrystals with highly energetic neutrons are modeled by adding to the thermal velocity of a predefined atom an extra contribution that accounts for the collision between such an atom and an incident neutron. This predefined atom is known in the literature as the

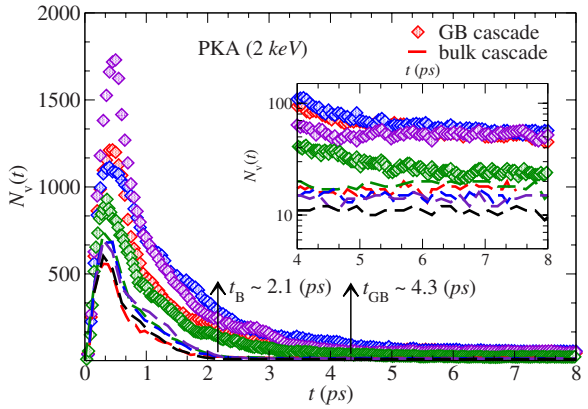

FIG. 2. (Color online) Evolution of the number of vacancies $N_v(t)$ over time for irradiated bulk samples (lines) and unstressed Fe bicrystals (symbols). For a given PKA energy, the transient t_B that characterizes the time and the meltlike region that lasts within the bulk is always smaller than the GB transient t_{GB}. The inset of the figure is a log-lin plot of the tails in order to better visualize the number of vacancies generated.

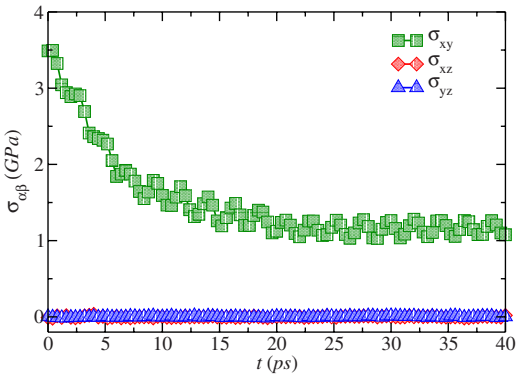

FIG. 3. (Color online) Stress relaxation in a symmetric tilt Fe bicrystal after its GB has been bombarded with a 1 keV PKA energy cascade. Initially, only the nondiagonal component in the plane of the applied strain xy is different from zero.

PKA. The energies characterizing such PKA collision events were found in the range 0.5–5 keV. Our bicrystals contain from 60 000 to 400 000 atoms. The reference system was formed by 60 000 atoms corresponding to box lengths of $L_x=L_y=127.6$ Å and $L_z=85.7$ Å. However, the box dimensions were increased up to $L_x=L_y=382.8$ Å and $L_z=428.3$ Å to ensure that there were no spurious boundary effects. In this work, whenever we refer to GB cascades, we are considering a simulation with the PKA located on the GB with the direction of its initial velocity oriented on the GB plane (yz plane in Fig. 1).

Last, to characterize the structural changes arising from primary radiation damage, we compute the time evolution of the number of vacancies $N_v(t)$. In the current bcc Fe systems, vacancy formation within the crystal can be ascertained by the $0.3a$ sphere criterion.[11] This criterion identifies vacancies as those perfect lattices sites not containing any atom within a sphere of radius $R=0.3a$ centered at the site. In Sec. III we present the results arising from the simulations.

III. RESULTS

In the absence of stress, grain boundaries and bulk material respond to displacement cascades in a qualitatively similar manner, although quantitative differences are observed. Analogous to bulk displacement cascades, a damage zone is created due to the collision avalanche which is centered near the GB PKA and peaks in our 2 keV incident PKA energy simulations at about 0.5 ps (Fig. 2). The displaced atoms in the outer region of the GB cascade return to their lattice positions more quickly whereas a meltlike disorder persists in the core for a few picoseconds. Self-interstitial atoms (SIA) and vacancies are then formed when the cascade core crystallizes.

Cascades at GBs are different as compared to bulk cascades in a number of ways. For instance, GB cascade meltlike cores last longer as compared to those in the bulk. In Fig. 2, we track the time evolution of the number of vacancies $N_v(t)$ as the simulations advance for nine different cases, five of which correspond to irradiated bulk samples. Note that the time t_B characterizing the duration of the meltlike region in the bulk is found to be smaller than the time t_{GB} characterizing the duration of the meltlike region at the GB for a given PKA energy. Furthermore, a larger number of vacancies is formed after crystallization of the GB cascade meltlike region and the time evolution of these vacancies shows greater fluctuations as compared to that of the bulk. Finally, a higher concentration of defects is found to be spatially distributed on the GB as recently reported by Samaras *et al.*[31,32] These results imply that GBs are more susceptible to PKA events and radiation damage than bulk material.

Below a certain threshold of combined internal stress and PKA energy, the nature of the processes occurring within irradiated bicrystals resembles that of unstressed systems. Conversely, above a threshold combination of internal stress and PKA energy, defects are nucleated at the GB, activating mechanisms which lead to stress relaxation via GB motion, i.e., sliding or migration. The activation of either sliding or migration depends on the nature of the internal stress. In our simulations, grain boundary migration is observed for nonzero internal stress component σ_{xy} whereas GB sliding is observed for nonzero internal stress component σ_{xz} (see Fig. 1 for axis orientation).

An example GB migration result is shown in Fig. 1, where an initial applied shear strain of $\gamma_{xy}=0.030$ and an incident PKA energy of 1 keV lead to an internal stress of $\sigma_{xy}=3.5$ GPa. Stress relaxation occurs as the boundary migrates toward the positive direction of the x axis (Fig. 3). In this particular example, the initial stress has been reduced by a factor close to 3 after equilibrating. A detailed characterization of the GB migration mechanism is provided within Appendix A. Concomitant migration and sliding[33] are observed in a number of our simulations. However, in the ensuing sections we focus on analyzing the simulation results which show GB sliding without migration.

A potentially more significant mechanism with regards to irradiation creep, which also leads to stress relaxation, is grain boundary sliding. An example of intrinsic grain boundary sliding, that is sliding in the absence of irradiation or

extrinsic GB point defects or dislocations, is initiated at an applied strain $\gamma_{xz}=0.045$, which results in an internal stress $\sigma_{xz}=5.2$ GPa. This intrinsic threshold condition can be compared to the results of Hyde *et al.*[23] who provided a comprehensive study of GB sliding in a $\Sigma=5$, (310)[001] bcc Fe symmetric tilt bicrystal. Hyde *et al.*[23] showed that an applied strain $\gamma_{xz}=0.065$ initiates GB sliding at 300 K. However, they also showed that this measured threshold shear strain is artificially increased when a small simulation box size is chosen for their simulations. We have also seen changes in the shear threshold with system size and have likely not used a large enough simulation box to fully eliminate this effect. Nevertheless, the main difference in threshold shear between our work and the study by Hyde *et al.* is likely due to differences in the EAM potentials employed.

While the intrinsic threshold stress for GB sliding in our case is $\sigma_{xz}=5.2$ GPa in the absence of radiation, we find that stresses as low as $\sigma_{xz}=3.8$ GPa can induce sliding during irradiation at $T=300$ K using a PKA with 1 keV energy. This represents a 27% reduction in the threshold internal stress. Thus, our simulations reveal that GB sliding is assisted via GB displacement cascades. These threshold conditions represent the minimum combination of internal stress which we observed to activate GB motion for a given PKA energy. Note however, that there exists an effective cutoff PKA energy below which the threshold internal stress is equal to that of the unirradiated case. Hyde *et al.*[23] reported that sliding in $\Sigma=5$ symmetric tilt bicrystals can occur by the nucleation and propagation of partial dislocations. The limiting step in the sliding process is the nucleation of partial dislocations of type $b=\pm\frac{1}{10}[310]$, which are found to nucleate homogeneously in the absence of point defects.[23] Hyde *et al.* showed that the introduction of a vacancy at the GB reduces the threshold internal shear stress (by 23% in their example) and acts as a site for heterogeneously nucleating GB dislocations. Therefore, we conclude that the introduction of irradiation defects at the GB, in the form of vacancies and SIAs, reduces the barrier to GB sliding by providing heterogeneous nucleation sites for generating GB dislocations.

Grain boundary sliding is quantified by computing the center of mass (com) of the crystal on both sides of the GB. An inelastic relative displacement Δz_{in} is estimated from the computed com by subtracting the initial relative displacement Δz_0 from the final relative displacement Δz_f. This initial relative displacement is primarily due to the initial applied elastic strain in the bicrystal. The GB sliding process is further analyzed by visualization using markers, several layers of atoms spaced along the z axis, which are assigned color depending on which side of the GB the atoms sit. In the presence of sliding, the relative position of the markers varies such that the lattice displacement on either side of the GB becomes easily identifiable (Fig. 4). The visualization supports a dislocation-based GB sliding mechanism, as a displacement front is observed to traverse the length of the GB during the primary stress relaxation.

A typical stress relaxation result is shown in Fig. 5. Incipient GB sliding is observed during the collision avalanche and is accompanied by slight stress relaxation (14% of the total). However, the bulk of the GB sliding occurs after the displacement cascade core has crystallized. This primary sliding is accompanied by a more significant stress relaxation (35% of the total) which is notably linear. In total, the internal stress relaxes from 3.8 to 2.0 GPa with a total relative inelastic displacement of $\Delta z_{\text{in}}=2.1$ Å. For this particular example, in Appendix B we have provided some complementary information related to how the initial temperature of the system affects the stress relaxation process.

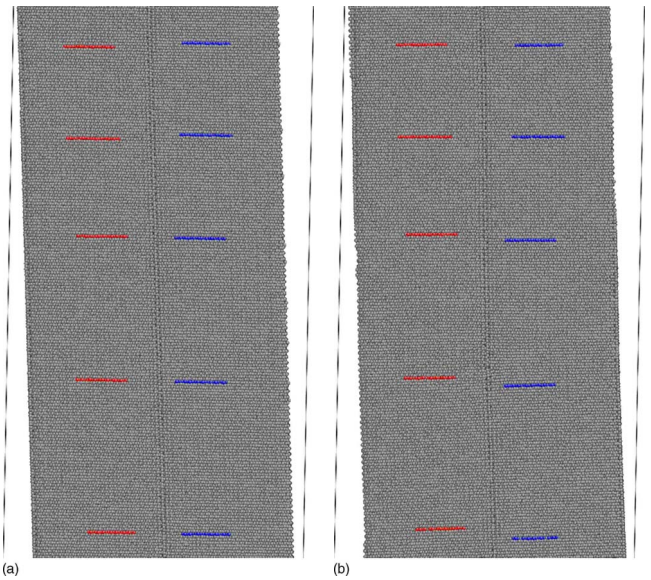

FIG. 4. (Color online) Visualization of the symmetric tilt bcc Fe bicrystal (a) before and (b) during GB sliding event under the action of a 2 keV GB displacement cascade. Several layers of marker atoms along the z axis were colored on both sides of the GB. After the cascade takes place, GB sliding can be identified by comparing the relative displacements of the markers.

More complex sliding responses for a given GB PKA energy can occur upon increasing the internal stress while still remaining below the intrinsic threshold value. For example, Fig. 6 shows the evolution of stress and relative com displacement with time for a bicrystal with an applied shear

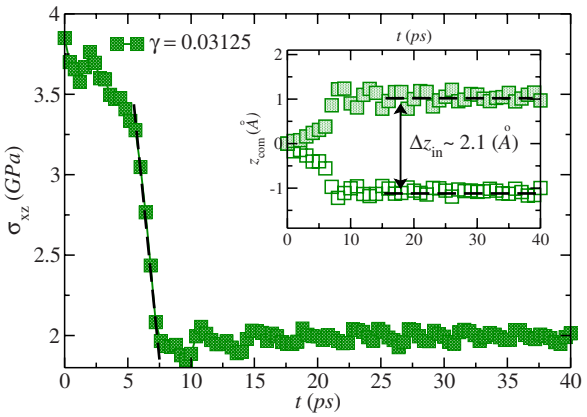

FIG. 5. (Color online) Stress relaxation for a Fe $\Sigma=5$, (310)[001] symmetric tilt bicrystal after being bombarded with a 1 keV GB cascade. The initial applied strain was $\gamma_{xz}=0.031$. The time evolution of the center of mass on both sides of the GB is shown in the inset plot.

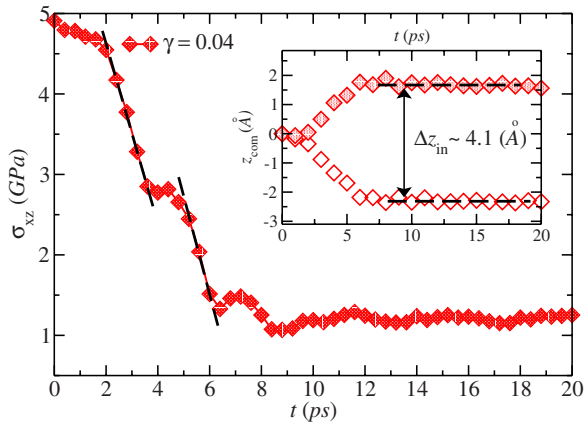

FIG. 6. (Color online) Stress relaxation for a Fe $\Sigma=5$, (310)[001] symmetric tilt bicrystal after being bombarded with a 1 keV GB cascade. The initial applied strain was $\gamma_{xz}=0.040$. The time evolution of the center of mass on both sides of the GB is shown in the inset plot.

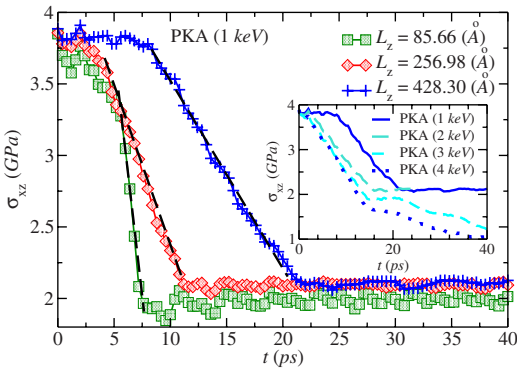

FIG. 7. (Color online) Relaxation of the stress component σ_{xz} of a tilt Fe bicrystal as a function of the size of the GB. Stress relaxes following a linear law via dislocation motion. Increasing the size of the boundary reduces the stress relaxation rate, conversely, increasing the PKA energy has no influence on such a variable (see inset). The inset plot relates to the case in which $L_z=428.30$ Å.

strain of $\gamma_{xz}=0.04$ and an incident GB PKA energy of 1 keV. The two-step stress relaxation process provides evidence for the activation of two equivalent inelastic sliding events. The primary stress relaxation events in Figs. 5 and 6 are characterized by $\Delta z_{\text{in}} \approx 2.0$ Å, a total stress relaxation of about 2.0 GPa, and a primary stress relaxation that is linear with time, which suggests that partial GB dislocations of the same character are emitted for all cases. It is possible that the nucleation and passage of the first GB partial dislocation restructure the GB and thereby lower the threshold stress required for activating the second GB partial dislocation.[23] For example, we note that the second partial dislocation is emitted at 2.75 GPa in Fig. 6, which is lower than the initial threshold of 3.8 GPa.

In the following, dislocation-induced GB sliding is characterized by providing an alternative analysis to the one reported by Hyde *et al.*[23] We note that the stress rate $d\sigma/dt$ follows a linear decay during the primary stress relaxation for the cases considered (Figs. 5 and 6). This finding is explored by considering the Orowan equation[34] for propagation-controlled dislocation motion, which relates the strain rate $d\gamma/dt$ and the average dislocation velocity $\langle v \rangle$ such that

$$\frac{d\gamma}{dt} = \rho_m b \langle v \rangle, \tag{1}$$

where ρ_m is the mobile dislocation density and b the absolute value of its Burgers vector. Using the relationship between stress and strain from linear elasticity theory, where $\sigma=\mu\gamma$ with μ being the shear modulus, the expression for the stress rate as a function of dislocation velocity is derived as

$$\frac{d\sigma}{dt} = \rho_m b \mu \langle v \rangle. \tag{2}$$

The average dislocation velocity $\langle v \rangle$ is usually considered a function of applied stress, which means that $d\sigma/dt$ is not expected to be constant. However, at high applied stress a saturation regime is reached where $\langle v \rangle$ is insensitive to stress.[35] For bcc Fe, the saturation velocity is approximately ≤ 0.7 of the smallest shear wave speed c_{min}, where $c_{\text{min}} \approx 25$ Å/ps. The $\langle v \rangle$ values obtained from the primary stress relaxation branches (i.e., $\langle v \rangle > 15$ Å/ps) in Figs. 5 and 6 suggest that stress relaxation occurs in the saturation regime where $\langle v \rangle \neq f(\sigma)$. Under these conditions, a constant $d\sigma/dt$ is consistent with Eq. (2).

We further explore the Orowan behavior by varying the GB length L_{GB} in the direction along which the dislocations travel, i.e., for $L_{\text{GB}}=L_z$ in this particular example. Figure 7 shows the stress relaxation results when L_{GB} is varied by up to a factor of 5. In all cases, constant $d\sigma/dt$ values are observed during the primary stress decay. In a separate set of simulations, we have examined the effect of increasing the incident PKA energy above the threshold value. The incident PKA energy should not significantly influence the primary stress relaxation, assuming the structure of the GB is not drastically altered due to the displacement cascade. The inset plot in Fig. 7 shows the stress relaxation results when the PKA energy is increased from 1 to 4 keV. As expected, incident PKA energy has little influence on $d\sigma/dt$ during primary stress relaxation (Fig. 7). However, as we only use NVE ensembles, increasing the PKA energy results in an increase in the system's temperature. A temperature increase should drive the system to smaller values of the equilibrium stress after relaxation occurs. This is indeed verified within the inset plot of Fig. 7.

The average GB dislocation velocity is calculated for the three cases presented in Fig. 7 using $\langle v \rangle = L_z/2t$. We obtain $\langle v \rangle$ equal to 15.8, 15.1, and 16.4 Å/ps. These nearly identical values support the idea of a unique dislocation mechanism driving GB sliding in $\Sigma=5$ symmetric tilt bicrystals, as the results are consistent with Eq. (2). Furthermore, Eq. (2) indicates that when $\langle v \rangle$ is constant and L_{GB} is varied, the data in Fig. 7 can be collapsed onto a single curve. This superposition is possible as ρ_m is inversely proportional to L_{GB}. Figure 8 demonstrates such a superposition where the time axis was rescaled such that $t=t_0+tL_{z_{\text{ref}}}/L_z$. Here t_0 is a time shift used to synchronize the initial stress relaxation and $L_{z_{\text{ref}}}$ is the length of the GB corresponding to our reference system. The

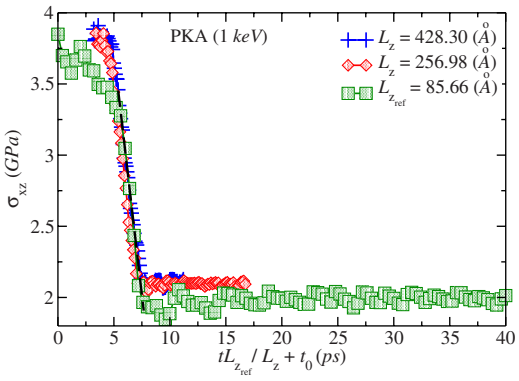

FIG. 8. (Color online) Superposition of the stress plots included within Fig. 7 by rescaling the time axis such that $t=t_0+tL_{z_{\mathrm{ref}}}/L_z$. t_0 represents a time shift employed to synchronize the starting of the stress relaxation in all cases and $L_{z_{\mathrm{ref}}}$ corresponds to the length of a reference GB.

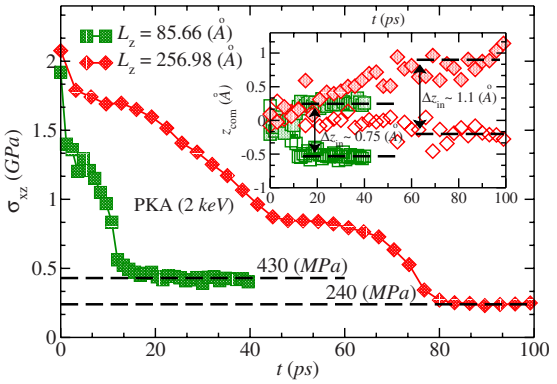

FIG. 9. (Color online) Relaxation of the stress component σ_{xz} of a Fe bicrystal after the action of a secondary GB cascade of 2 keV. The initial status of the system corresponds to two of the relaxed configurations shown in Fig. 7. The inset plot shows the corresponding sliding due to the second cascade. The coms are centered about the origin as we have subtracted from both the average initial coms because the GBs considered within this set of calculations had different lengths.

reference configuration has $L_{z_{\mathrm{ref}}}=85.66$ Å and corresponds to the smallest GB shown in Fig. 7.

As materials in nuclear reactors are irradiated for long times, we also investigated how consecutive GB displacement cascades influence GB sliding and stress relaxation. We are interested in how structural change and disorder, introduced into the GB due to the primary GB cascade event and passage of the partial dislocations, change the GB stability and resistance to further radiation damage. To address such a question, previously irradiated bicrystals were used as input for a new set of GB displacement cascade simulations. The PKAs used to initiate the secondary GB displacement cascades were randomly selected.

The results show that secondary GB cascades initiate GB sliding at much lower internal stress than that observed in the primary displacement cascade simulations. Significant stress relaxation is also observed. For example, the application of a 2 keV incident PKA reduces the internal stress from 2 GPa to 430 and 240 MPa for the two cases presented in Fig. 9. The lowered GB sliding threshold stress is primarily due to GB restructuring caused by the passage of partial dislocations during the primary relaxation (as discussed by Hyde *et al.*[23]) and the increased disorder created by the secondary GB displacement cascade. Furthermore, the stress relaxation data in Fig. 9 cannot be normalized to produce a master curve. This suggests that the operative dislocation sliding processes for both simulations are not equivalent, even though the starting configuration for both simulations is a $\Sigma=5$ symmetric tilt bicrystal irradiated with 2 keV incident PKA. Evidently, the stochastic nature of the first GB displacement cascade event, where the PKA is chosen randomly, influences further irradiation damage and the GB sliding observed in the secondary simulations. Finally, a lack of marked linearity in $d\sigma$ versus dt suggests that $\langle v\rangle=f(\sigma)$. The increased sensitivity of $\langle v\rangle$ with internal stress is possible due to the increased density of GB point defects which provide obstacles to GB dislocation motion and the lowered internal stress.

In relation to the calculations of overlapping cascades presented in the above paragraph, we would like to bring the reader's attention to the fact that in a real experiment the time between consecutive cascades is much larger than any MD time (on the order of milliseconds). Therefore in between two cascades many migration processes can occur (particularly of self-interstitials) which could change significantly the final damage of the cascade obtained from MD simulations.

The irradiation-assisted GB migration and sliding observed in the current work are mechanisms which likely aid creep processes in irradiated materials, especially those materials with a high volume fraction of grain boundaries and interfaces. The defects and structural disorder present at GBs in polycrystalline materials are likely to lead to the nucleation of GB dislocations under much smaller internal stresses than those encountered in the ideal $\Sigma=5$ symmetric tilt bicrystal studied in the current work. Irradiation-assisted GB sliding may also enhance irradiation creep by providing a mechanism which aids the accommodation of intragranular deformation processes. We believe that the role of GBs in irradiation-assisted creep is likely to be significant, and perhaps even dominant, in real materials. GBs provide a mechanism by which the point defects induced by irradiation can lead directly to stress relaxation. In bulk regions away from GBs or dislocations, the only mechanism for this relaxation would seem to be the coalescence of radiation-induced vacancies into mobile dislocation loops, which seems likely to be a much slower process of stress relaxation than what we have described here. Unpinning of dislocations due to irradiation damage is another potentially significant source of stress relaxation in these systems. The nature of irradiation-assisted creep in polycrystals is a topic we are currently investigating.

IV. SUMMARY

Molecular-dynamics simulations have been used to investigate the influence of displacement cascades on the stability of a symmetric $\Sigma=5$ tilt grain boundary in bcc Fe. In the

absence of internal stress, GBs are found to be more susceptible to displacement cascade damage than the defect-free lattice. This result motivated us to study the combined influence of GB displacement cascades (those which envelop the GB) and internal stress on GB structure and stability.

A threshold combination of internal stress and incident PKA energy was found to activate GB motion, which takes the form of migration or sliding depending on the nature and magnitude of the internal stress. In particular, we find that grain boundary radiation damage lowers the threshold stress required to activate grain boundary motion. Our results, coupled with the detailed mechanistic study of Hyde *et al.*[23] allow us to postulate that the defects created by the grain boundary displacement cascade act as heterogeneous sites for the nucleation of GB dislocations, which then drive the GB sliding process.

The dislocation-mediated GB motion leads to significant stress relaxation, which is shown to be consistent with the Orowan equation for dislocation-induced strain. Last, we studied the action of consecutive GB cascades as we are interested in how structural change and disorder, introduced into the GB due to the primary GB cascade event and the subsequent GB sliding, change the GB stability and resistance to further radiation damage. We find that the structural changes at the GB due to the passage of the first set of partial dislocations, coupled with defects and disorder created by the secondary cascade, lead to a lower GB sliding threshold stress and further stress relaxation. We note that irradiation-assisted GB sliding is a mechanism which potentially aids creep processes in irradiated materials, especially in those materials with a high volume fraction of grain boundaries and/or interfaces.

ACKNOWLEDGMENTS

We wish to acknowledge the Office of Energy Research and Development (OERD) at Natural Resources Canada for providing funding for this project. The Atlantic Computational Excellence Network (ACEnet) is also acknowledged for assisting us with computational resources. C.C. gratefully thanks NSERC for making the collaboration with CANMET-Materials Technology Laboratory possible.

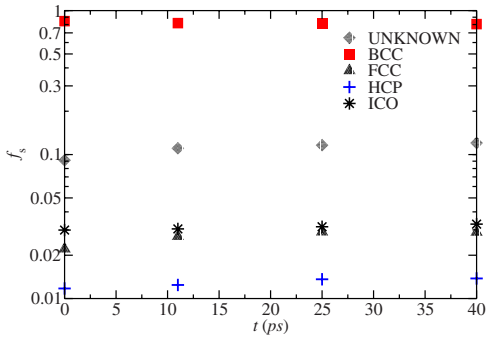

FIG. 10. (Color online) The time evolution of the ratio f_c of atoms belonging to each type of lattice structure according to the algorithm of Ackland and Jones (Ref. 36) is shown in the figure. The algorithm proved to be successful when identifying crystal structures on slightly strained (sheared) simulation boxes.

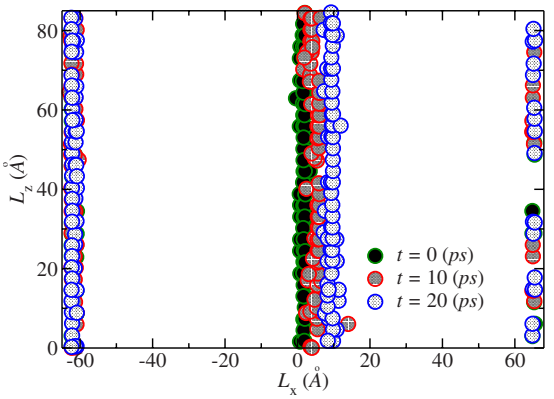

FIG. 11. (Color online) An algorithm proposed by Ackland to identify crystalline structures is used to track the migration of the GB from Fig. 1. Only the atoms labeled as hcp coordinated are plotted.

APPENDIX A: GB MIGRATION CHARACTERIZATION

To characterize GB migration, we compute the GB boundary velocity vm_{GB} by using Ackland and Jones[36] algorithm to automatically track GB position. The algorithm identifies local crystal structure for the bcc, fcc, hcp, and icosahedral (ico) Bravais lattices by comparing lattice angle distributions. To test the algorithm of Ackland and Jones on stressed bicrystals, we have calculated the ratio of atoms f_c belonging to each of the four lattice systems cited above. Figure 10 shows the evolution of f_c as the GB displayed in Fig. 1 migrates. The algorithm registers $f_c \approx 0.85$ for the bcc structure, which is remarkably good considering that the algorithm of Ackland and Jones was developed for identifying local lattice structures in stress and defect-free crystals.

The GB velocity can then be calculated by recognizing that hcp atoms are only detected at the GB. Figure 11 visualizes the position of the hcp atoms as the GB migrates in the direction of the positive x axis. The GB position is then used with the corresponding GB migration time to estimate vm_{GB}. In the example shown in Fig. 11, we obtain $vm_{GB} \approx 0.5$ Å/ps.

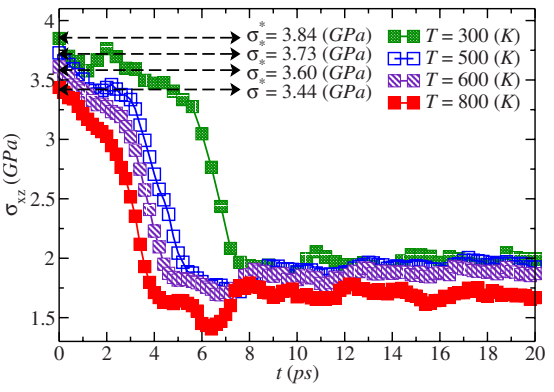

FIG. 12. (Color online) Temperature effects on the stress relaxation in a symmetric tilt Fe bicrystal after its GB has been bombarded with a 1 keV PKA energy cascade. Increasing the temperature of the bicrystal reduces its intrinsic stress threshold σ^*. Higher temperatures also ensure lower values of the equilibrium stress after the relaxation process has happened.

APPENDIX B: TEMPERATURE EFFECTS

The results of increasing (decreasing) the initial temperature within our simulations are briefly covered in this appendix. For this purpose, the same system used to generate Fig. 5 was initialized such that its temperature was chosen to be located in the range $300 \leq T \leq 800$ K. Next, a 1 keV GB cascade was induced and the stress relaxation of the system was recorded as shown in Fig. 12.

Three main features arise as the initial temperature of the bicrystal increases. First, the intrinsic stress threshold σ^* becomes smaller. Such a behavior matches perfectly the observations of Hyde *et al.*[23] Second, GB sliding via dislocation motion remains as the prominent mechanism for stress relaxation for temperatures of up to $T=800$ K. Last, the higher the initial temperature the lower the final equilibrium stress reached by the system. This last observation agrees with classical thermodynamics, as an increase in the temperature of the material increases the transition probability between different states of the internal degrees of freedom. Consequently, when a relaxation process occurs, the system corresponding to the highest temperature will have reached a lower stress configuration within the stress landscape.

*Corresponding author; rmiller@mae.carleton.ca

[1] A. T. R. for Generation IV Nuclear Energy Systems, U.S. DOE Nuclear Energy Research Advisory Committee and the Generation IV International Forum No. GIF-002-00, 2002.
[2] V. Ghetta, D. Gorse, D. Mazire, and E. V. Pontikis, *Materials Issues for Generation IV Systems: Status, Open Questions and Challenges* (Springer, Dordrecht, The Netherlands, 2008).
[3] F. A. Garner, M. B. Toloczko, and B. H. Sencer, J. Nucl. Mater. **276**, 123 (2000).
[4] S. M. Bruemmer, E. P. Simonen, P. M. Scott, P. L. Andresen, G. S. Was, and J. L. Nelson, J. Nucl. Mater. **274**, 299 (1999).
[5] T. Diaz de la Rubia, H. M. Zbib, T. A. Khraishi, B. D. Wirth, M. Victoria, and M. J. Caturla, Nature (London) **406**, 871 (2000).
[6] C. C. Fu, J. D. Torre, F. Willaime, J. L. Bocquet, and A. Barbu, Nature Mater. **4**, 68 (2005).
[7] A. F. Calder and D. J. Bacon, J. Nucl. Mater. **207**, 25 (1993).
[8] N. Soneda and T. D. de la Rubia, Philos. Mag. A **78**, 995 (1998).
[9] R. E. Stoller, J. Nucl. Mater. **276**, 22 (2000).
[10] B. D. Wirth, G. R. Odette, J. Marian, L. Ventelon, J. A. Young-Vandersall, and L. A. Zepeda-Ruiz, J. Nucl. Mater. **329**, 103 (2004).
[11] A. Souidi, C. S. Becquart, C. Domain, D. Terentyev, L. Malerba, A. F. Calder, D. J. Bacon, R. E. Stoller, Y. N. Osetsky, and M. Hou, J. Nucl. Mater. **355**, 89 (2006).
[12] M. Samaras, P. M. Derlet, H. V. Swygenhoven, and M. Victoria, J. Nucl. Mater. **351**, 47 (2006).
[13] D. A. Terentyev, T. P. C. Klaver, P. Olsson, M. C. Marinica, F. Willaime, C. Domain, and L. Malerba, Phys. Rev. Lett. **100**, 145503 (2008).
[14] D. J. Bacon and Y. N. Osetsky, Int. Mater. Rev. **47**, 233 (2002).
[15] L. Malerba, J. Nucl. Mater. **351**, 28 (2006).
[16] M. Victoria *et al.*, Fusion Eng. Des. **82**, 2413 (2007).
[17] G. J. Ackland, J. Nucl. Mater. **351**, 20 (2006).
[18] A. Caro, D. A. Crowson, and M. Caro, Phys. Rev. Lett. **95**, 075702 (2005).
[19] D. A. Terentyev, L. Malerba, R. Chakarova, K. Nordlund, P. Olsson, M. Rieth, and J. Wallenius, J. Nucl. Mater. **349**, 119 (2006).
[20] J.-H. Shim, H.-J. Lee, and B. D. Wirth, J. Nucl. Mater. **351**, 56 (2006).
[21] http://lammps.sandia.gov
[22] S. J. Plimpton, J. Comput. Phys. **117**, 1 (1995).
[23] B. Hyde, D. Farkas, and M. J. Caturla, Philos. Mag. **85**, 3795 (2005).
[24] J. D. Rittner and D. N. Seidman, Phys. Rev. B **54**, 6999 (1996).
[25] J. Nocedal and J. S. Wright, *Numerical Optimization* (Springer-Verlag, New York, 1999).
[26] A. Caro and M. Victoria, Phys. Rev. A **40**, 2287 (1989).
[27] M. W. Finnis, P. Agnew, and A. J. E. Foreman, Phys. Rev. B **44**, 567 (1991).
[28] A. M. Rutherford and D. M. Duffy, J. Phys.: Condens. Matter **19**, 496201 (2007).
[29] M. I. Mendelev, S. Han, D. J. Srolovitz, G. J. Ackland, D. Y. Sun, and M. Asta, Philos. Mag. **83**, 3977 (2003).
[30] Y. Qi and P. E. Krajewski, Acta Mater. **55**, 1555 (2007).
[31] M. Samaras, P. M. Derlet, H. Van Swygenhoven, and M. Victoria, Phys. Rev. Lett. **88**, 125505 (2002).
[32] M. Samaras, P. M. Derlet, H. V. Swygenhoven, and M. Victoria, Philos. Mag. **83**, 3599 (2003).
[33] M. Shiga and W. Shinoda, Phys. Rev. B **70**, 054102 (2004).
[34] D. Hull and D. J. Bacon, *Introduction to Dislocations* (Pergamon, New York, 1984).
[35] D. L. Olmsted, L. G. Hector, Jr., W. A. Curtin, and R. J. Clifton, Modell. Simul. Mater. Sci. Eng. **13**, 371 (2005).
[36] G. J. Ackland and A. P. Jones, Phys. Rev. B **73**, 054104 (2006).